

Comparison of activity of three low-cost adsorbents for the removal of methylene blue dye – optimization using central composite design-response surface methodology

Sangeetha Jayaraman, R Sharmil Suganya, Thiruvengadam Venugopal*

Department of Chemistry, Government College of Engineering, Salem-11, India, emails: t.venu1973@gmail.com (T. Venugopal), sangeethaj2009@gmail.com (S. Jayaraman), sweetsharmil@gmail.com (R Sharmil Suganya)

Received 12 November 2022; Accepted 12 May 2023

ABSTRACT

Three activated carbon was prepared from *Prosopis cineraria* (PCAC) barks, seeds of *Ocimum basilicum* (OBAC), and pods of *Tecoma stans* (TSAC) using phosphoric acid activation. Fourier-transform infrared spectroscopy (FTIR) analysis shows that all the activated carbon has a similar functional group and the FTIR spectrum of the activated carbon after adsorption indicates the effective removal of methylene blue (MB) by the activated carbon. Brunauer–Emmett–Teller analysis of the activated carbon shows its high surface area and pore size ideal for the removal of MB dye. Response surface methodology with the central composite design model was applied and the optimized condition for the removal of MB was obtained. Experimental optimized removal of 91.5% was obtained for PCAC at a concentration of 254 ppm, duration 33.3 min and temperature 326.4 K, 92% removal at a concentration of 233 ppm, duration 31.6 min and temperature of 326.4 K, for OBAC and 93.4% removal at a concentration of 255.9 ppm, duration 41.9 min and temperature 326.4 K for TSAC. The adsorption was found predominantly physical by all the activated carbon and endothermic. Freundlich isotherm was predominately followed for the removal of MB. Second-order kinetics and Webber–Morris model were found to be followed by all the carbon.

Keywords: Adsorption; Isotherm; Kinetics; Optimization; Thermodynamics

1. Introduction

Methylene blue (MB) (3,7-bis(dimethylamino)-phenothiazin-5-ium chloride) is a cationic heterocyclic aromatic dye – containing thiazine. It is widely used in cotton and silk industries [1]. About 10% of MB and other pollutants discharged from the industry can affect the environment severely and also it is non-biodegradable [2]. Long-term continuous contact with MB leads to harmful effects. If decomposed under certain conditions, it produces more than 20 kinds of carcinogenic aromatic amines [3]. Methylene blue dye reduces the penetration power of light into water bodies and consequently reduces the photosynthesis process [4]. Ingesting methylene blue orally, leads to vomiting,

nausea, methemoglobinemia and damage to the nervous system [5,6,7]. Inhalation of MB leads to difficulty in breathing, also, contacting with eyes leads to permanent eye problems for humans and animals [8].

Even low concentrations of dyes also can harm living organisms in water streams. Therefore, it must be treated before use. The adsorption technique using activated carbon is more widely used to remove the organic pollutants present in the water than the other competitive techniques like degradation, coagulation, membrane, oxidation, and ion exchange [9,10]. This study aims in removing the MB dye by adsorption using three low-cost activated carbon prepared by the simple activated method. The study helps to find the optimized condition for the removal of the MB

* Corresponding author.

dye using the central composite design-response surface methodology (CCD-RSM) technique. The study was also used to find the best-activated carbon for the removal of MB dye from wastewater.

2. Material and methods

2.1. Preparation of adsorbate

Prosopis cineraria barks were collected from the Rasipuram, Tamil Nadu, *Ocimum basilicum* seeds were obtained from Kollu Hills, Tamil Nadu, and the pods of *Tecoma stans* (TSAC) were obtained from Salem, Tamil Nadu. The raw plant material was washed thoroughly with distilled water to remove adhering dust and impurities, dried, ground, and sieved to fine particles. Powdered material was soaked in 50% H_3PO_4 at a ratio of 4:1 (acid in mL: powder material in g) and kept in an oven for 1 h at 80°C. Acid-impregnated material was carbonized in a tube furnace under a nitrogen atmosphere. It was heated to 650°C with 1 h holding time. After cooling to room temperature, the activated carbon was washed thoroughly with distilled water until the filtrate became neutral and then it was dried in an oven at 100°C for about 8 h. The resulting activated carbon was ground, sieved, and kept in desiccators for further use.

2.2. Preparation of dye

Methylene blue was obtained from Qualigens Fine Chemicals, Mumbai. The stock solution of the pollutants was prepared in distilled water. 1 g of dye was dissolved in 1,000 mL DD, containing a 1,000 ppm dye concentration. It was diluted by adding a suitable amount of distilled water.

2.3. Characterization and analysis

The instruments used in this study were UV-Vis Spectrophotometer (ELICO SL-159) for the analysis of dyes, scanning electron microscopy (SEM, ZEISS EVO LS 15, Germany), energy-dispersive X-ray spectroscopy, Fourier-transform infrared spectroscopy (FTIR, PerkinElmer Version 10.03.09) for the characterization of the sorbent, Brunauer-Emmett-Teller (BET) instrument (NOVA, Quantachrome® ASiQwin™, Quantachrome Instrument Version 3.0) to determine the surface area and porosity measurements under liquid nitrogen atmosphere and AERIS-PANalytical instrument for powder X-ray diffraction (XRD) analysis of the samples.

Measurements were carried out using the general traditional photometry method at a maximum wavelength over-working solution concentration. The efficiency was checked with different time intervals and marked by every 10 min of time interval using an UV-Vis Spectrophotometer (ELICO SL-159 Model). A blank was also used. The effect of temperature on the adsorption of PCAC, OBAC, and TSAC was evaluated in the range of 298–328 K by contacting 100 mL of contaminated solution with a definite initial concentration of 0.1 g of adsorbent materials. The experiments were also performed in the initial pH range of 2–10, and the initial pollutant concentration range of 50–200 mg/L. The amount of adsorption at equilibrium time q_e (mg/g) was calculated from Eq. (1).

$$q_e = \frac{(c_0 - c_e)v}{w} \quad (1)$$

where c_0 is the concentrations of adsorbate at initial, c_e is concentrations at equilibrium state (mg/L) and v , w are the volume of sample solution (L) and the weight of the adsorbent (g), respectively.

2.4. Response surface methodology

RSM is a combination of many statistical techniques used to optimize the process for obtaining the desired response by the interaction of some variables. Statistical design helps to reduce the number of experiments [11]. RSM is used to identify, optimize and enhance the operating conditions [12]. The optimization and modeling techniques approach one at a time, RSM and ANN the artificial neural network methods. RSM can be applied to perform a variety of experimental designs. Hence, CCD was selected as the best design to perform the experiments and estimate the coefficients in a mathematical form in order to predict the response and validation of the model [13]. CCD is a suitable model for fitting the entire surface, which gives better results with a minimum number of experiments for taking decisions [14–16].

Experimental factors like independent variables such as initial pollutant concentration, adsorbent dose, temperature, and solution pH can be optimized for removal efficiency of dyes (MB, RB, and R6G) and heavy metal Cr removal by RSM/CCD was carried out by MINITAB 20.3. RSM comprises the following classes hybrid design, Box-Behnken design (BBD), CCD, and three-level factorial design. CCD uses a fractional factorial design while BBD uses a spherical three-level design. BBD has only the central point and the middle point of the circle in the sphere. BBD does not require extreme conditions and the sphere is around the maximum and minimum limit of the variable. The CCD was a well appropriate design for fitting quadratic surfaces, which works well for process optimization.

The replicates in the center point were considered to determine the precision of the experiments in the removal of dye. In the design, out of 20 runs, 6 runs are repeated at the center point. The experimental data from CCD are fitted to the second-order polynomial equation to establish a relationship between the responses and various variables. Eq. (8) was developed by the software from the behavior of the system:

$$Y = \beta_0 + \sum \beta_i X_i + \sum \beta_{ii} X_i^2 + \sum \beta_{ij} X_i X_j \quad (8)$$

where β_0 , β_i , β_{ii} , and β_{ij} are offset term, linear effect, squared effect and interactive effect, respectively.

A three – factor 5 – level CCD ($-\alpha, -1, 0, +1, +\alpha$) was used in the DOE for the RSM. The number of runs in the CCD is 20 and the α for the design is 1.682. The CCD design for the 3 (k) variable has a 2^k cube point of 8, the center point in the cube is $2k$ of 6, and the axial point of 6. R -square value was used to determine the fitness of the model and a 95% confidence level of R -square was acknowledged. The efficiency of the model was determined using F -values

also. The model's statistical significance and variables were determined at the 5% probability level ($P < 0.05$). The CCD program also demonstrated the analysis of variance (ANOVA) based on F and P -values. The model was plotted in a response profile. A response function was used to fix the best-operating conditions of the process.

3. Results and discussion

3.1. Characterization of adsorbent after the adsorption of MB

3.1.1. Scanning electron microscopy

The structural morphology based on the pre and post adsorption of MB dye on the adsorbents of PCAC, OBAC, and TSAC has been analyzed using SEM as shown in Fig. 1. It indicates that the PCAC, OBAC, and TSAC carbons have good porosity and high adsorption capacity. The SEM images of the activated carbon has a large number of voids of different sizes. The surface of all the activated carbon was found to be porous and rough. Molecular diffusion onto the surface can easily take place on a rough porous surface rather than on a non-porous, smooth surface. Hence, activated carbon used in this study with porous and rough textures can highly facilitate molecular diffusion of the dye onto the surfaces [17]. The SEM images of activated carbon after the adsorption of MB dye shows a large decrease in the porous nature which in-turn indicates the complete and efficient adsorption of the dye onto the surface.

3.1.2. Fourier-transform infrared spectroscopy

The surface functional groups of PCAC, OBAC, and TSAC, before and after adsorption were determined by FTIR as shown in Fig. 2. Adsorption bands were observed at $3,450\text{--}3,400\text{ cm}^{-1}$ (PCAC: $3,422$, OBAC: $3,415.5$, and TSAC: $3,426\text{ cm}^{-1}$) corresponding to --OH stretching vibration of various types of hydroxyl groups. A peak is seen around $2,900\text{ cm}^{-1}$ corresponding to asymmetric C--H stretching. The shift of the peak from $1,575$ to $1,595\text{ cm}^{-1}$ of PCAC, the new

sharp peak at $1,592\text{ cm}^{-1}$ of OBAC, and the peak at $1,587\text{ cm}^{-1}$ of TSAC represented the formation of $\pi\text{--}\pi$ interaction between the aromatic rings of MB and C=C of all the adsorbents. The newly observed peaks at around $1,300\text{--}1,100\text{ cm}^{-1}$ shown by all the adsorbents can facilitate the removal of MB from the solution. The obtained peak at $1,381$; $1,376$ and $1,382\text{ cm}^{-1}$ of PCAC, OBAC, and TSAC, respectively shows the presence of --OH bending of carboxylic acid, the peaks at $1,325$; $1,314$ and $1,316\text{ cm}^{-1}$ indicates the presence of C--N group of MB, respectively. A newly appeared small peak at 873 cm^{-1} of PCAC, 875 cm^{-1} of OBAC, and 896 and 820 cm^{-1} of TSAC assigned the aromatic C--H of MB. The presence of the --S group of MB corresponds to the peaks at $1,019$; $1,024$ and $1,022\text{ cm}^{-1}$ of PCAC, OBAC, and TSAC, respectively after the adsorption of MB proved the presence of MB on the surface of all the adsorbents, respectively.

3.1.3. X-ray diffraction

The XRD analysis of the compound indicates whether the sample is crystalline or amorphous or both in the same sample [18]. Fig. 3 shows the XRD result of the activated carbons PCAC (a), OBAC (b), and TSAC (c), respectively. The XRD analysis confirms the amorphous structure of all the activated carbons due to the broadband at 23° and 43° . This band corresponds to the disordered stacks of graphite layers. Hence it was considered to be in disorder and of graphitization form. The peak on these angles corresponds to (002) and (100) planes which indicates reflection like graphite. Higher peak intensity for all the activated carbon at 2θ around 23° indicates stacks of the parallel layer of carbon present. The d_{002} plane values are shown in Table 1 and the values are between $0.369\text{--}0.372\text{ nm}$. The value of the d_{002} plane indicates a disordered framework of structure since the value of the (002) plane is higher than 0.335 nm for ideal crystalline graphitization. OBAC shows two peaks in the 2θ of 24° and for each peak, the lattice parameter and the interplanar distance were found. The peak at 2θ around 43° indicates an orderly structure but the intensity of these

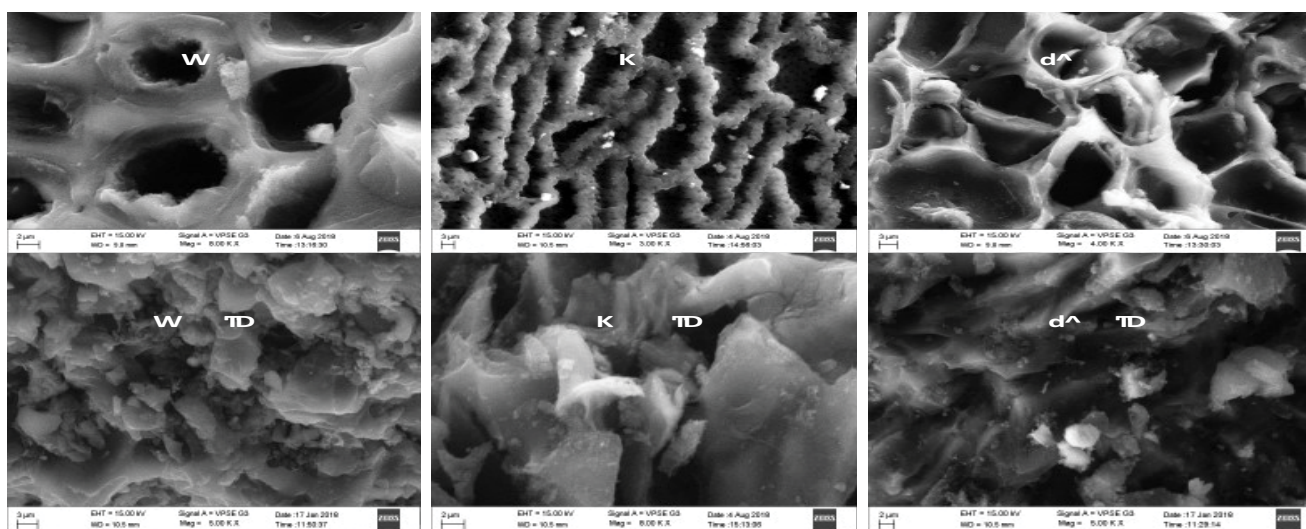


Fig. 1. Scanning electron microscopy images of PCAC, OBAC, and TSAC before and after the adsorption of methylene blue.

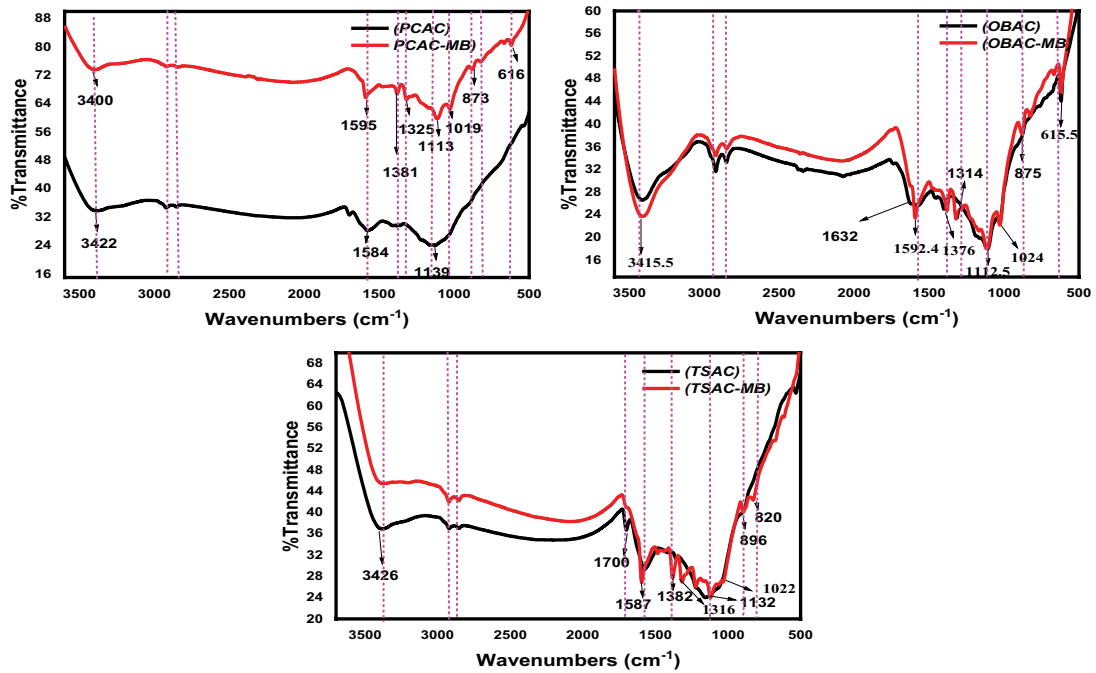


Fig. 2. Fourier-transform infrared spectroscopy of adsorbents before and after adsorption of methylene blue.

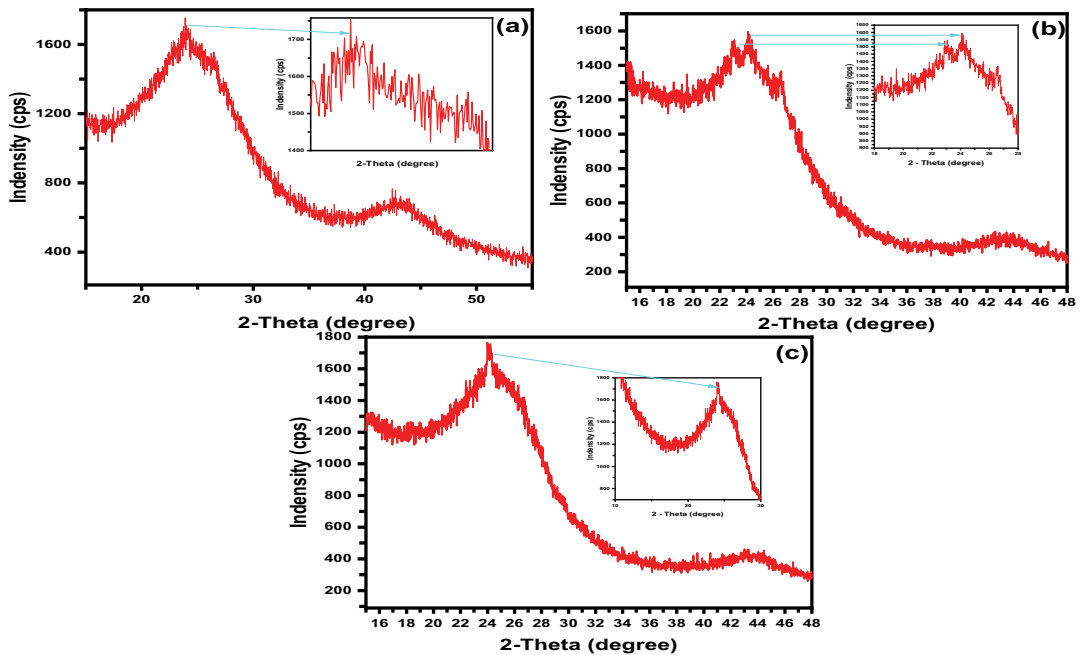


Fig. 3. X-ray diffraction of PCAC, OBAC and TSAC.

peaks is far lesser than the peak at 23°, hence, the amorphous nature of the carbon is confirmed. These types of peaks are shown by activated carbon prepared by phosphoric activation and other activation methods. Lattice parameters L_c and L_a were calculated from the peak intensity using Origin 8.0 software and is shown in Table 1. It can be seen from the table that L_a value for all the carbon was higher than the L_c value indicating the growth of crystals in the

plane and disordered carbon getting incorporated into the graphite-like layers.

3.1.4. Brunauer–Emmett–Teller

The N_2 adsorption/desorption isotherms of activated carbons are shown in Fig. 4. Table 2 shows the surface area, pore size, and total pore volume of PCAC, OBAC, and

Table 1
Microcrystalline parameter and interlayer spacing of PCAC, OBAC, and TSAC

	X-ray data				Microcrystalline parameters (nm)		Effective dimension (nm)
	$2\theta_{(002)}$ (deg.)	$2\theta_{(100)}$ (deg.)	d_{002} (nm)	d_{100} (nm)	L_c	L_a	L'
PCAC	23.87	42.45	0.372	0.213	0.28	0.60	0.365
OBAC P1	24.09	42.63	0.369	0.212	0.0177	0.038	0.0231
OBAC P2	23.07		0.385		0.0177		
TSAC	23.99	43.02	0.371	0.210	0.228	0.491	0.299

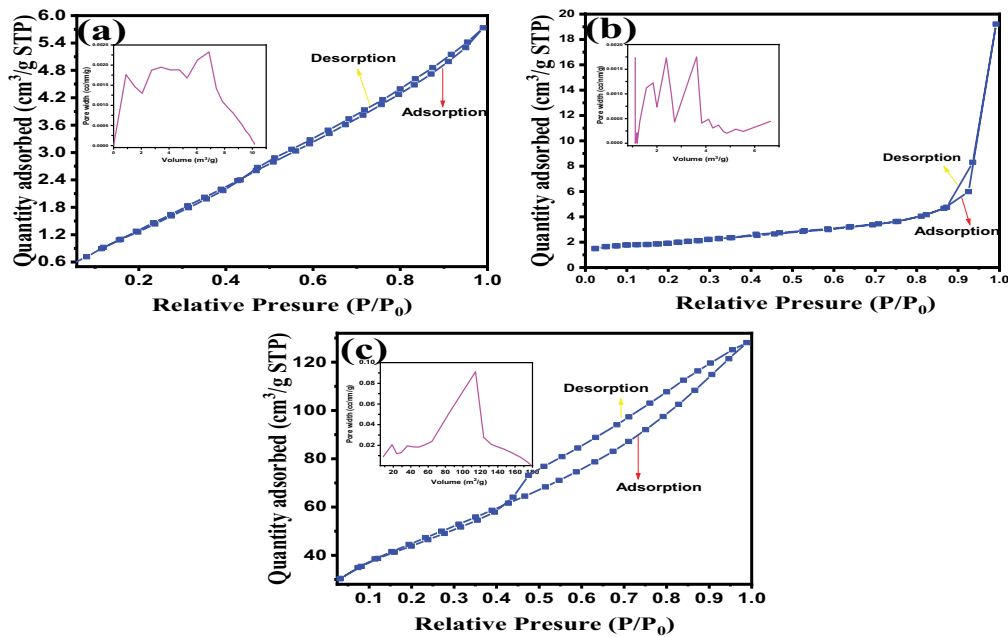


Fig. 4. Brunauer–Emmett–Teller – N_2 adsorption/desorption isotherm (a) PCAC, (b) OBAC and (c) TSAC.

Table 2
Brunauer–Emmett–Teller surface area, pore diameter, and pore volume

Adsorbent	Brunauer–Emmett–Teller surface area (m^2/g)	Pore diameter (nm)	Pore volume (cc/g)
PCAC	7.024	3.63	0.01
OBAC	6.664	3.11	0.012
TSAC	161.911	3.665	0.195

TSAC, respectively. From BET analysis of activated carbon, it was found that the surface area value of PCAC, OBAC, and TSAC was 7.024, 6.664, and 161.911 (m^2/g) with a pore volume of 0.01, 0.012, and 0.195 (cc/g), the pore diameter of 3.63, 3.11 and 3.665 (nm), respectively. The average pore diameter for the activated carbon was approximately 30 Å (>2 nm) which belongs to the mesoporous range [17,19]. The choice of activating agent for the preparation of activated carbon is found to be deciding factor for the size of

the pore. Activated carbon prepared by the phosphoric acid activation has been reported to form a mesoporous structure compared to other activation like $ZnCl_2$ which form a microporous structure [20]. TSAC has been found to have the highest pore diameter but with the largest surface area. The pore diameter of the activated was found to be ideal for the adsorption of methylene blue. The ideal pore size required for the adsorption of the dye is between 1.7 to 6 times the size of the MB. The size of the MB is 13 Å and all the activated carbon was found to have a size between 1.7 to 6 times the size of the MB. When the size of the pore is less than the size of the dye, the molecule cannot pass through the pore and the adsorption would be poor [21]. The type of adsorption curve followed by the activated carbon was found to differ from one another. PCAC, OBAC and TSAC were found to follow the types II, III and IV, respectively.

3.1.5. Adsorption experiments

3.1.5.1. Effect of contact time and initial concentration of MB

The efficiency of MB dye adsorption from the contaminated aqueous solution depends on the initial dye

concentration and contact time. The adsorption quantity (uptake of MB) increases with an increase in both of the parameters. The removal percentage of MB dye by PCAC, OBAC, and TSAC was decreased with increasing initial dye concentration and increased with contact time. The steady increase in the adsorption of MB with PCAC, OBAC, and TSAC till the equilibrium was attained is shown in Fig. 5. After the existence of an equilibrium state the diffusion of dye molecule slows down without affecting the rate of adsorption due to repulsion between adsorbed and unadsorbed adsorbate molecules present in the solution [22]. Effect of concentration studies for MB dye adsorption on PCAC, OBAC, and TSAC revealed that an equilibrium was attained in 40 to 60 min at 100 mg/L. For this reason, all the experiments were carried out for 180 min to ensure reaching equilibrium. Removal percentage of MB onto PCAC, OBAC, and TSAC at equilibrium was found that 95.8%, 96.56%, and 99.1% at an initial dye concentration of 100 mg/L, pH 10, and 328 K, and no change was found after the attainment of equilibrium.

3.1.5.2. Effect of temperature

Fig. 6 shows the adsorption isotherms of MB on PCAC, OBAC, and TSAC at temperatures of 298, 308, 318, and 328 K. The effect of temperature indicates whether the process is endothermic or exothermic. The rise in temperature will increase the adsorption capacity if it is an endothermic process and it will decrease if it is an exothermic process. By using the fixed solution concentration of 100 mg/L at different temperatures (298, 308, 318, and 328 K), the adsorption of MB from synthetic solution was evaluated. The adsorption increased slightly by increasing the temperature. Due to the higher temperature, a decrease in the solution viscosity leads to more diffusion of ions into the adsorbent pores and was responsible for maximum adsorption [23,24]. The adsorption efficiency of MB dye with 100 mg/L concentration increased from 91% to 95.8%, 86.54% to 96.55%, and 90% to 99% on the adsorbents PCAC, OBAC, and TSAC when the temperature is increased from 298 to 328 K and

at high-temperature, time taken for the equilibrium to be reached also decreases. It revealed that the adsorption was favored by increasing temperature. Moreover, it represents that the adsorption of MB onto all the adsorbents was an endothermic process.

3.1.5.3. Effect of solution pH

The adsorption of MB on PCAC, OBAC, and TSAC was studied in different pH ranges of dye solution (2–10) as shown in Fig. 7. The study of pH was used to explain the mechanism of interaction between the adsorbent materials and the applied dyes. The surface charge has an important role in this mechanism. Solution pH can alter the charge of the adsorbent surface. The adsorption capacity was increased by increasing the pH value from 2 to 10. At a high solution pH value, the solid surface possessed negative charges. Hence, at pH 10, MB had high electrostatic attraction with the negatively charged surface of the solids, thereby the pH increases, the number of sites that have negative charges increases and vice versa. At pH 10 the adsorption percentage of MB was found to be 95.8%, 96.55%, and 99% on PCAC, OBAC, and TSAC in the dye concentration of 100 mg/L at 328 K. Therefore, the optimum pH range for high amount of MB removal from aqueous solution was 7–10 over PCAC, OBAC, and TSAC. According to the effect of the concentration of dye solution temperature and pH, the order of removal efficiency of MB for activated carbons was found to be TSAC > OBAC > PCAC.

3.1.5.4. Adsorption isotherms

The study of isotherm was used to determine the total amount of adsorbent needed to adsorb a required amount of dye in the solution [25]. Table 3 gives the parameter for the model of the isotherm. The fit of isotherm models to the experimental data is represented in Figs. 8–10. Table 4 summarizes the isothermal constants' calculated parameters for the different tested models. The best fit for each

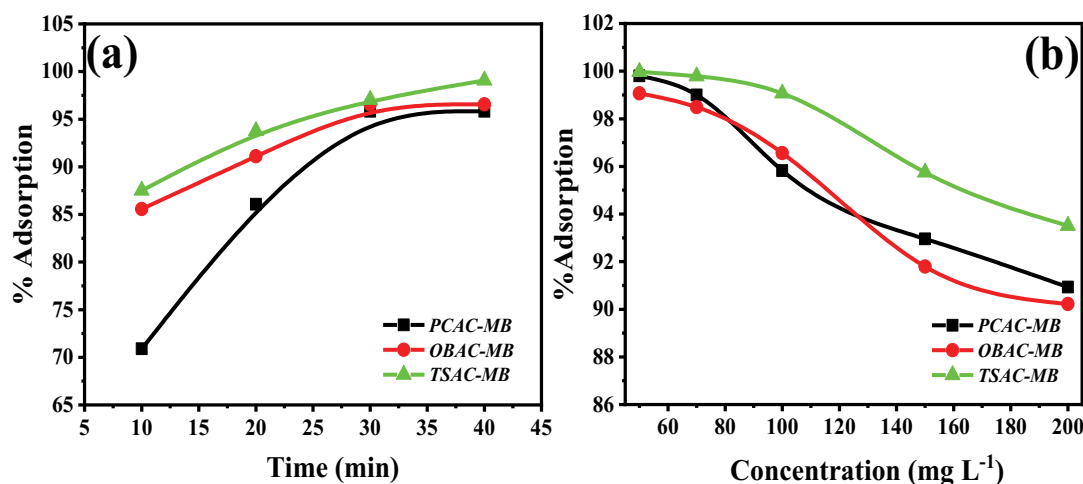


Fig. 5. Effect of contact time (100 mg/L) and effect of initial concentration (50–100 mg/L) on the removal of methylene blue dye at pH 10, and 328 K.

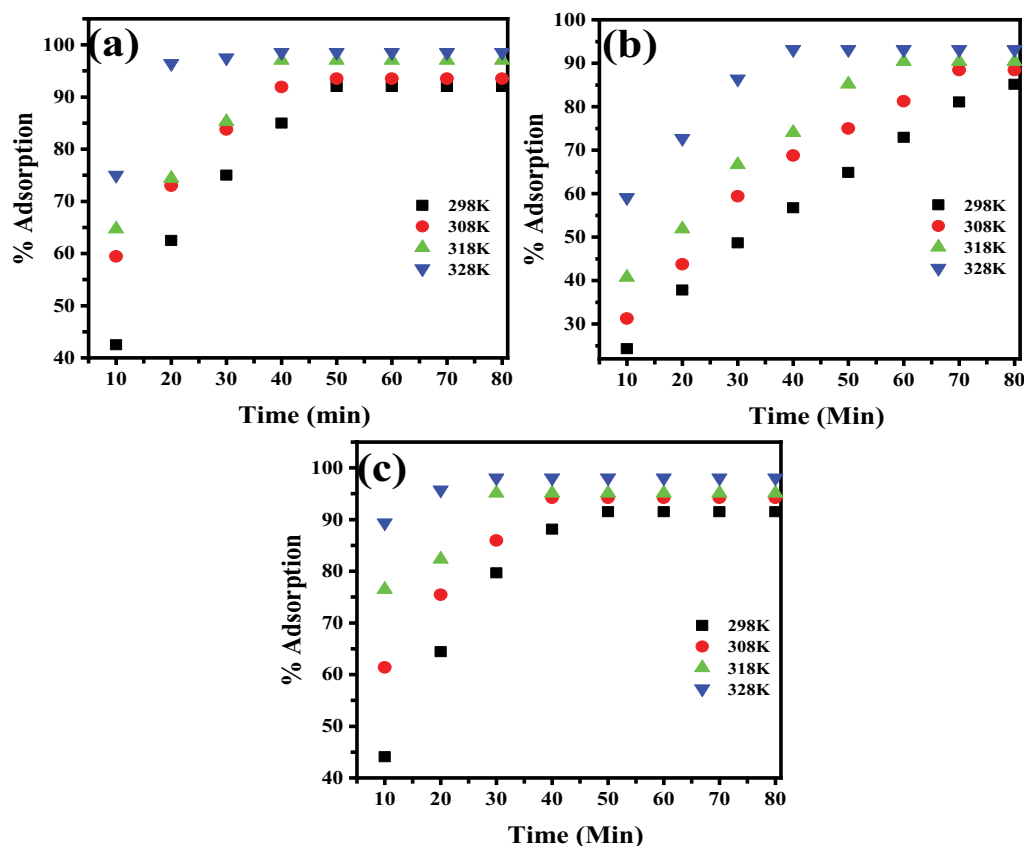


Fig. 6. Effect of temperature for the adsorption of methylene blue.

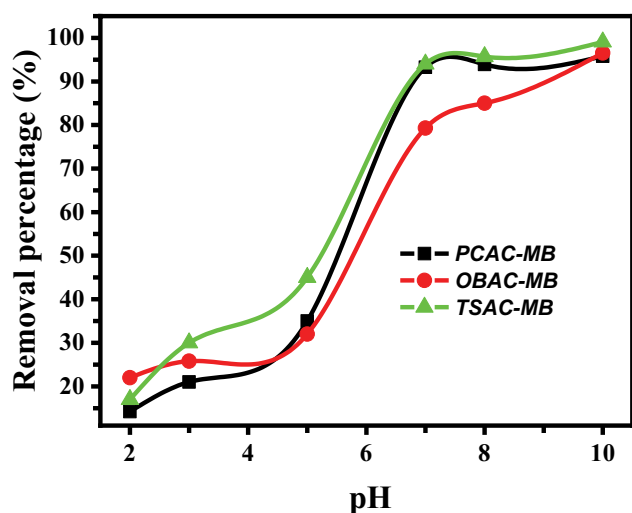


Fig. 7. Effect of pH.

isotherm model was evaluated in terms of the distribution coefficient (R^2).

Langmuir proposed model is applicable to the physical adsorption of a monolayer on a homogeneous surface. It is related to the maximum adsorption capacity in the monolayer. The maximum adsorption capacity means the occupation of adsorbate molecules on all the available surfaces

of the adsorbent. According to this model, each molecule possesses constant enthalpies and activation energy but there is no interaction between them.

Freundlich's empirical formula applied to multilayer adsorption did not restrict the monolayer formation. Freundlich isotherm analyses the adsorption of solutes in heterogeneous pores of adsorbents. The heterogeneous surface has unequal heat of adsorption and affinities. This model explains reversible and nonideal adsorption. Freundlich constants like K_F (adsorption capacity) and $1/n$ (degree of heterogeneity) represents the maximum adsorption capacity (mg/g) and the adsorption intensity [26]. The heterogeneity factor $1/n$ value lies between 0 and 1 indicating that the process is favorable. The obtained ' n ' values are greater than unity (2.16–5.18) at all the working temperatures indicating that the adsorption was desirable on the heterogeneous surface of all the adsorbents. In Table 2, the linear equation of Freundlich gives the better model describing the adsorption of MB by giving higher R^2 for all three carbons. The adsorption capacity, K_F calculated from the slope of the Freundlich plot for PCAC, OBAC, and TSAC were 34.57, 28.16, and 45.57 L/g, respectively.

When solution concentration is neither low nor high, the Temkin model assumes the heat of adsorption and characterizes the distribution of molecules on the surface of the adsorbents. In Eq. (4), B and A is related to the heat of adsorption and equilibrium binding constant of Temkin isotherm, respectively. Regression analysis of the

Table 3
Equations for isotherm and kinetic models

S. No.	Models	Linear form	Linear plot	Equations
1	Langmuir isotherm	$\frac{C_e}{Q_e} = \frac{C_e}{Q_m} + \frac{1}{K_L \cdot Q_m}$	$\frac{C_e}{q_e}$ vs C_e	(2)
2	Freundlich isotherm	$\log Q_e = \log K_F + \frac{1}{n} \log C_e$	$\log Q_e$ vs $\log C_e$	(3)
3	Temkin isotherm	$Q_e = B \ln A_T + B \ln C_e$	Q_e vs $\ln C_e$	(4)
4	Pseudo-first-order	$\log(Q_e - Q_t) = \log Q_e - \frac{K_1}{2.303} t$	$\log(Q_e - Q_t)$ vs t	(5)
5	Pseudo-second-order	$\frac{t}{Q_t} = \frac{1}{K_2 Q_e^2} + \frac{1}{Q_e} t$	$\frac{t}{Q_t}$ vs t	(6)
6	Webber–Morris model	$Q_t = K_{id} \sqrt{t} + C$	Q_t vs \sqrt{t}	(7)
7	Parameters of the models	Eq. (2): where Q_m = monolayer adsorption capacity (mg/g); C_e = equilibrium concentration of adsorbate (mg/L); K_L = Langmuir constant related to the energy of adsorption (L/mg) Eq. (3): K_F = Freundlich constant (approximate indicator adsorption capacity); n = adsorption intensity Eq. (4): Temkin constants; B = heat of adsorption; A_T = binding energy (L/g) Eq. (5): Q_t = adsorption capacity at time t (mg/g); K_1 = first-order rate constant Eq. (6): K_2 = second-order rate constant (mg/g·min) Eq. (7): Webber–Morris constants viz.; K_{id} = intraparticle diffusion rate constant (mg/g·min ^{1/2}); C = thickness of the boundary layer (mg/g)		

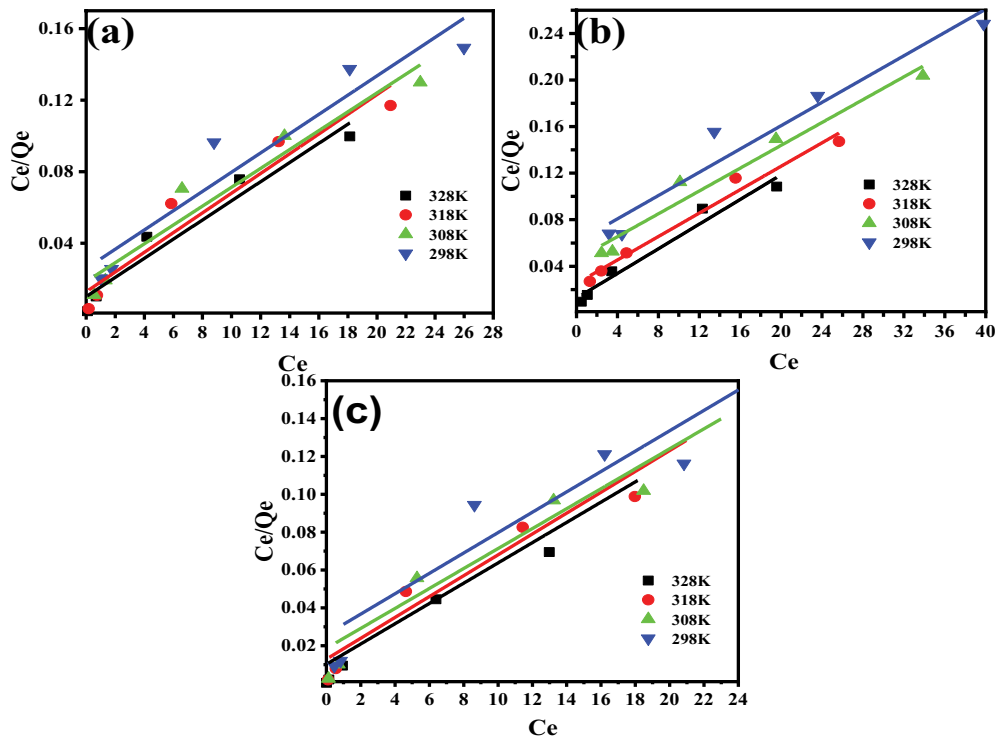


Fig. 8. Langmuir model for methylene blue adsorption on PCAC, OBAC, and TSAC.

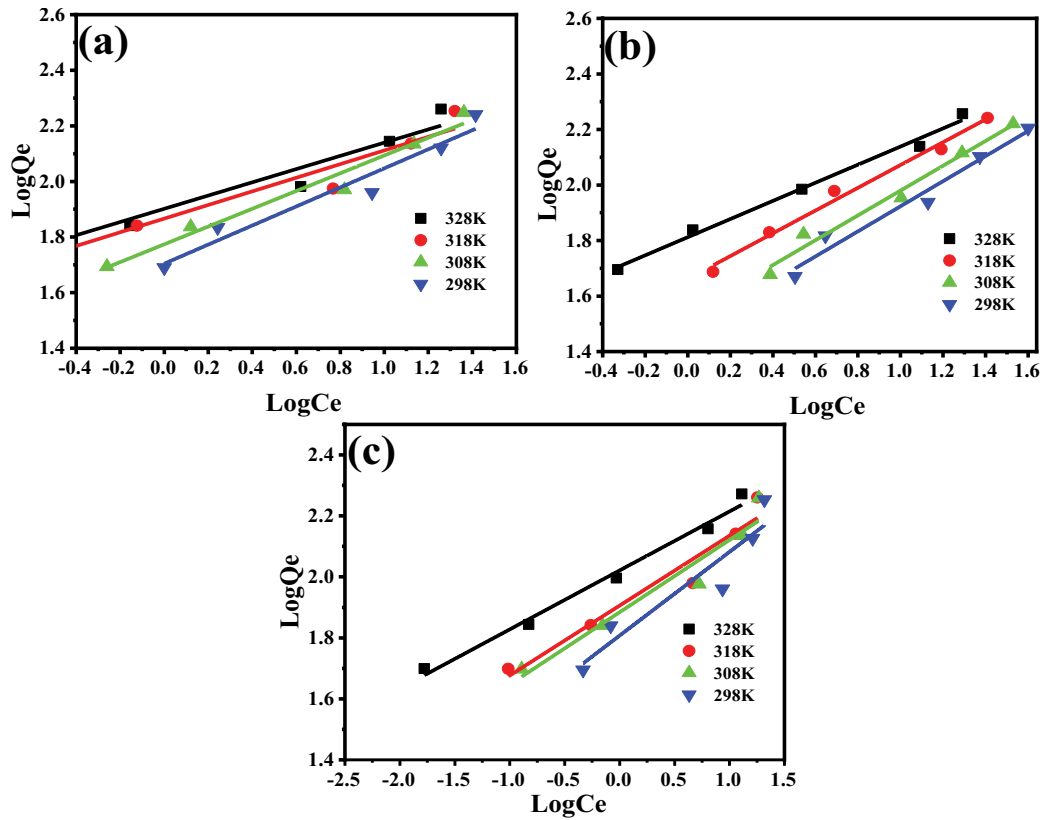


Fig. 9. Freundlich model of methylene blue adsorption.

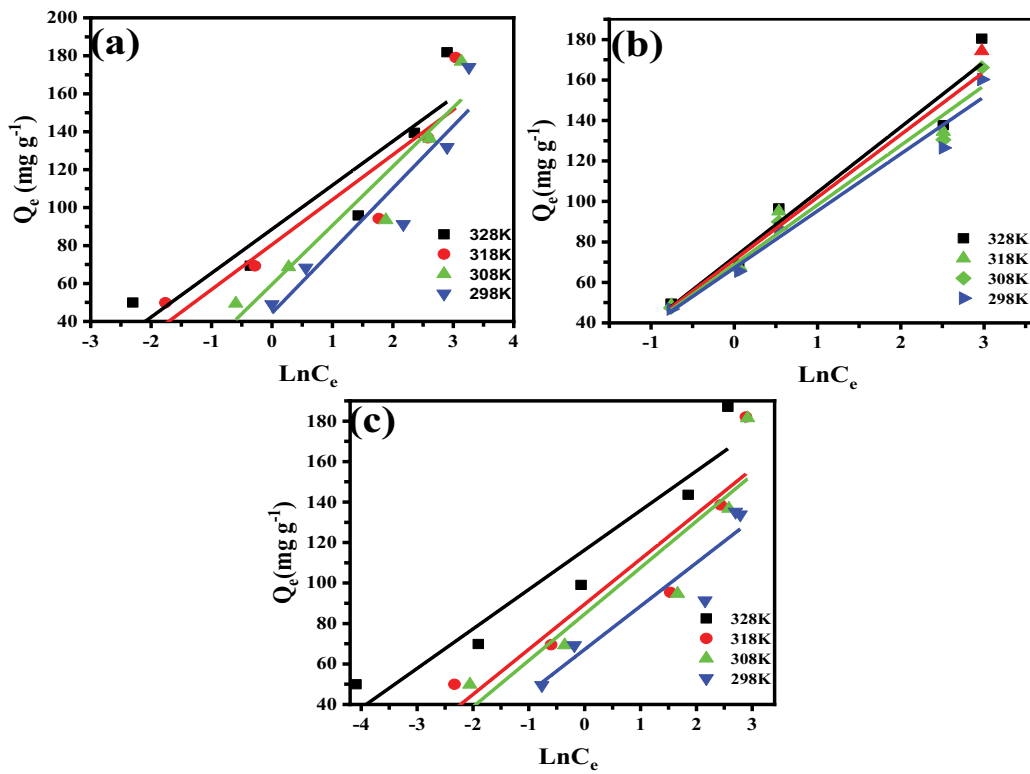


Fig. 10. Temkin isotherm model of methylene blue adsorption.

Table 4
Isotherm parameters of PCAC, OBAC, and TSAC for different temperatures

Adsorbent	Temp. (K)	Langmuir			Freundlich			Temkin		
		Q_m (mg/g)	K_L (L/mg)	R^2	K_f (L/g)	n	R^2	A	B	R^2
PCAC	328	200	0.5	0.949	34.57	4.2	0.951	45.84	23.16	0.851
	318	250	0.093	0.932	15.09	2.16	0.945	29.96	23.67	0.847
	308	200	0.278	0.939	25.75	3.13	0.967	6.798	31.06	0.896
	298	200	0.2	0.917	21.96	2.92	0.948	3.862	32.87	0.879
OBAC	328	200	0.417	0.967	28.16	3.07	0.991	9.48	32.18	0.958
	318	200	0.2	0.979	19.89	2.44	0.988	2.28	40.47	0.978
	308	250	0.089	0.966	14.78	2.24	0.979	1.19	42.36	0.959
	298	200	0.083	0.948	12.84	2.22	0.968	1.08	41.54	0.941
TSAC	328	200	1.667	0.98	45.57	5.18	0.987	388	19.5	0.916
	318	200	0.5	0.937	34.89	4.37	0.944	55.5	22.29	0.84
	308	200	0.455	0.927	33.24	4.22	0.937	40.2	22.91	0.827
	298	200	0.714	0.977	36.79	3.72	0.891	23.2	21.37	0.885

Table 5
Kinetic parameters

Adsorbent	Temperature (K)	Pseudo-first-order			Pseudo-second-order			Webber–Morris		
		Q_1 (mg/g)	K_1	R^2	K_2	H	R^2	K_{id}	C	R^2
PCAC	328	155.414	-0.16	0.945	0.00114	17.85714	0.998	10.81	37	0.997
	318	144.6191	-0.106	0.756	0.00096	11.9048	0.959	9.135	32.5	0.918
	308	121.648	-0.077	0.739	0.00079	9.80392	0.966	8.311	30.62	0.949
	298	106.076	-0.063	0.822	0.00069	8.54701	0.978	7.589	30.3	0.973
OBAC	328	22.20775	-0.07	1	0.00386	47.619	0.998	4.726	70.41	0.995
	318	23.5807	-0.051	0.98	0.00289	35.7143	0.997	4.246	67.54	0.984
	308	33.8306	-0.035	0.995	0.00159	15.873	0.989	5.651	47.81	0.969
	298	65.2514	-0.061	0.873	0.00116	11.6279	0.993	6.137	39.64	0.992
TSAC	328	28.40022	-0.087	0.996	0.00426	52.6316	0.999	3.673	76.48	0.978
	318	28.4571	-0.091	0.924	0.00526	52.6316	0.999	3.264	75.07	0.981
	308	48.101	-0.081	0.988	0.00188	23.2558	0.999	6.973	51.95	0.951
	298	57.413	-0.096	0.987	2.4E-05	24.3902	0.999	5.688	54.11	0.882

Langmuir (C_e/q_e vs. C_e), Freundlich ($\ln C_e$ vs. $\ln q_e$), and Temkin ($T^{1/2}$ vs. q_e) parameters of constants and the correlation coefficients are presented in Table 4. The Freundlich parameters resulted in high correlation coefficients of 0.917–0.991 (R^2), indicating a strong positive relationship.

3.1.5.5. Adsorption kinetics

Kinetic models such as pseudo-first-order, second-order, and intraparticle diffusion methods were described to study the rate and mechanism of the adsorption process based on the concentration of the solution over the entire time range. The constant parameters (as given in Table 3) for each model are shown in Table 5. In the pseudo-first-order model, by plotting the values of $\log(q_e - q_t)$ vs. t (Fig. 11), the value of k_1 and q_e can be determined from the slope and intercept of the obtained line, respectively. The validity of the model is checked by the correlation coefficient (R^2) and

closeness of calculated equilibrium adsorption capacities to the respective experiment value. According to the R^2 value examined, the pseudo-first-order model is not suitable for all experimental data.

The sorption data were checked by the plot of t/q_t vs. t (Fig. 12) for the pseudo-second-order kinetic model and it gives a straight line with a high correlation coefficient the k_2 and equilibrium adsorption capacity (q_e) was calculated from the intercept and slope of this line, respectively. The high values of R^2 for the adsorption of MB dye (0.991, 0.999, and 0.985 of PCAC, OBAC, and TSAC, respectively) and closeness of experimental and theoretical adsorption capacity (q_e) values for all responses shows the applicability of the pseudo-second-order model to explain and interpret the experimental data (Table 5). Finally, the process possibility is investigated using the Webber–Morris model (intraparticle diffusion). The plot of q_t vs. $t^{1/2}$ (Fig. 13) gives K_{diff} the intraparticle diffusion

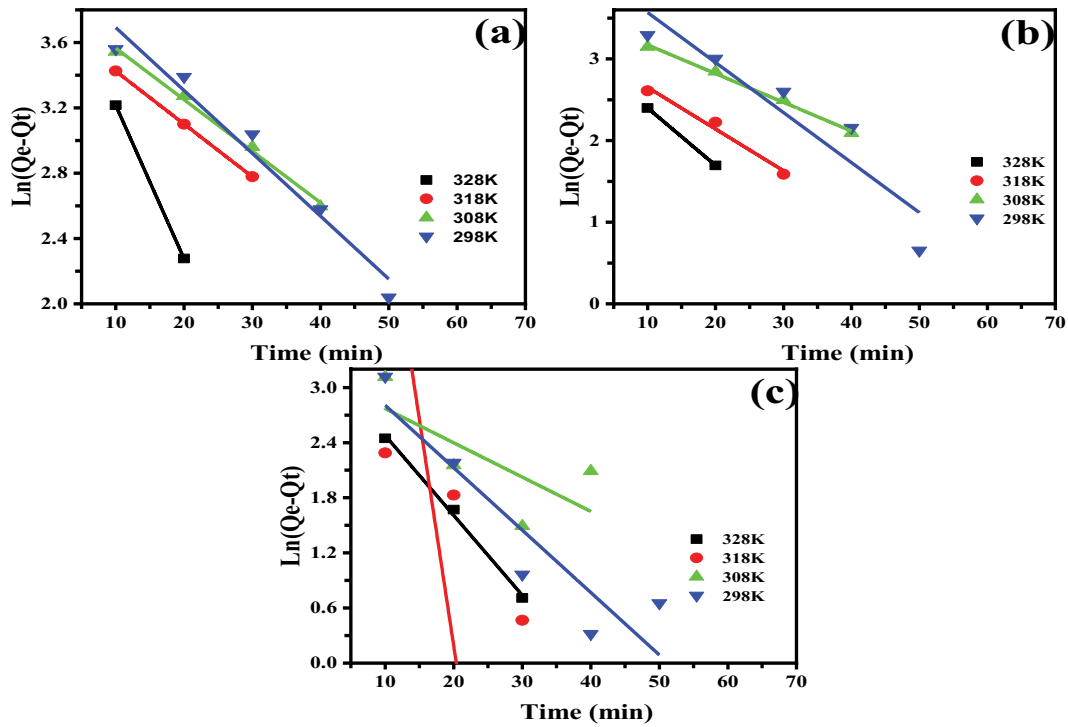


Fig. 11. Pseudo-first-order kinetics.

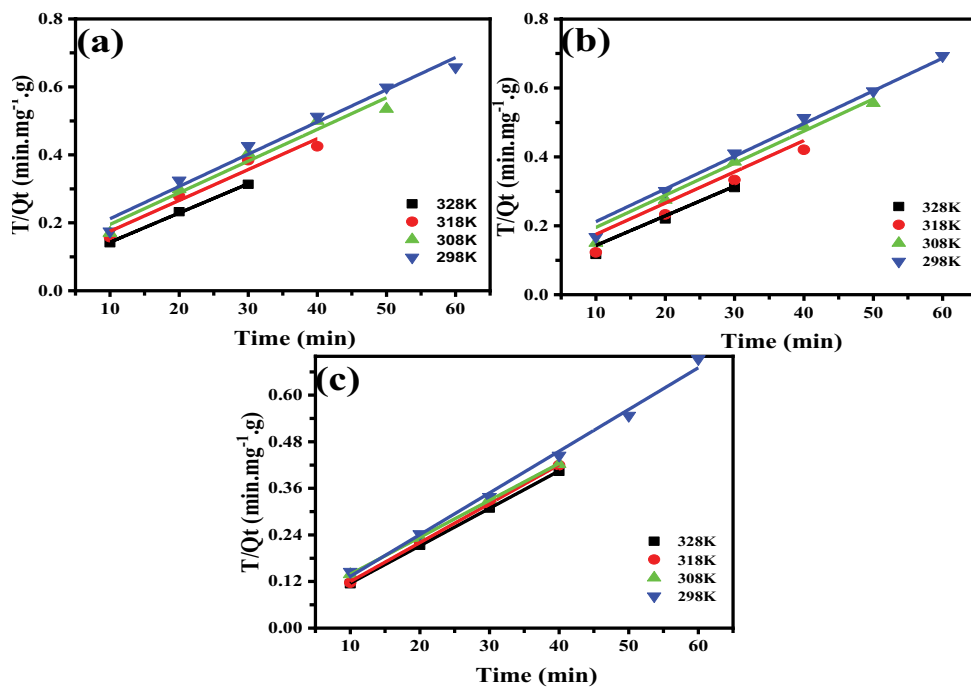


Fig. 12. Pseudo-second-order kinetics.

rate constant (mg/g.min^{1/2}) from the slope and the intercept gives C (the layer thickness) for MB dye. The corresponding model fitting parameters (shown in Table 5) indicates the adsorption mechanism and also follows the intraparticle diffusion process for simultaneous adsorption process.

3.1.5.6. Thermodynamic studies

The thermodynamic parameters indicates the practical application of the adsorption process. Each thermodynamic parameter with its signs reveals that the effect of temperature of the process such as Gibbs free (ΔG°) energy

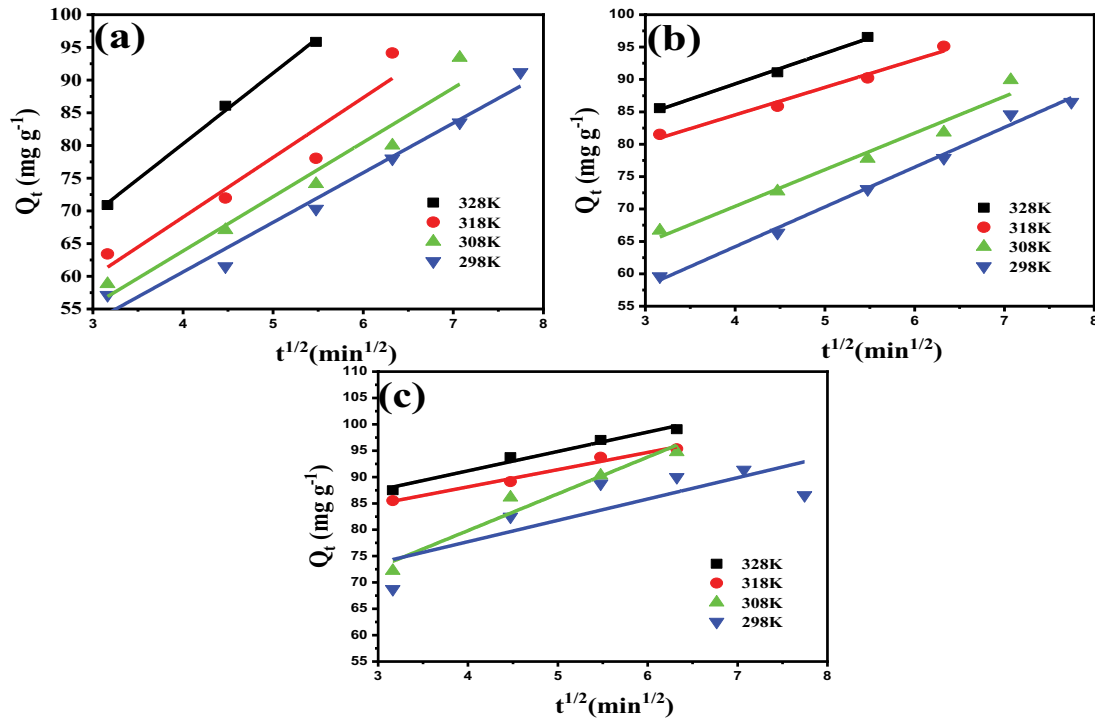


Fig. 13. Webber–Morris model.

change indicates the spontaneity of the process, enthalpy change reveals the nature of the process, and the entropy change indicates that the disorder of ions in the surface of adsorbents. All these parameters can be calculated from the linear form of the Van't Hoff Eqs. (9)–(11).

$$\Delta G^\circ = -RT \ln K_c \quad (9)$$

$$K_c = \frac{Q_e}{C_e} \quad (10)$$

$$\ln K_c = -\frac{\Delta H^\circ}{RT} + \frac{\Delta S^\circ}{R} \quad (11)$$

where K_c is the equilibrium constant (L/g), R is the gas constant (8.314 J/mol·K), T is the absolute temperature in Kelvin, Q_e is the amount of adsorption at equilibrium time (mg/g) and C_e is the equilibrium concentration (mg/L). ΔG° is the Gibbs free energy change (kJ/mol), ΔH° is the enthalpy change (kJ/mol) and ΔS° is the change of entropy (J/mol).

Thermodynamic parameter obtained in the process at different temperature was summarized in Table 6 for 100 mg/L of dye solution. The data was plotted on a graph with $\ln K_{eq}$ on the Y-axis vs. $1/T$ on the X-axis. In the plot, $-\Delta H^\circ/R$ is the slope and $\Delta S^\circ/R$ is the intercept of the linear fit. Knowing the slope and intercept from the plot (Fig. 14) ΔH° and ΔS° values can be easily determined using:

$$\Delta H^\circ = -\text{slope} \times R \quad (12)$$

$$\Delta S^\circ = \text{intercept} \times R \quad (13)$$

Table 6
Thermodynamic parameters

Adsorbent	Temp. (K)	Thermodynamic parameters			
		ΔG° (kJ/mol)	ΔH° (kJ/mol)	ΔS° (J/mol·K)	R^2
PCAC	328	-8.54327			
	318	-7.34405	20.33604	87.7127	0.969
	308	-6.79032			
	298	-5.79603			
OBAC	328	-9.09003			
	318	-7.84579	42.1936	156.469	0.97
	308	-5.59785			
	298	-4.61015			
TSAC	328	-12.7086			
	318	-7.9936	56.5685	207.85	0.818
	308	-7.39391			
	298	-5.84783			

The positive value of ΔH° (20.33604 for PCAC, 42.1936 for OBAC, and 56.5685 for TSAC, respectively) confirms that the process was endothermic ($\Delta H^\circ > 0$), and also the obtained ΔH° values are less than 84 (kJ/mol) [27] which represents that the adsorption is physisorption. The positive value of ΔS° indicates the increase in disorder at the adsorbent/adsorbate interface during the process. The release of the solvent molecules during the adsorption may increase the entropy of the system. The negative value of ΔG° reveals that the process was spontaneous within the range of

temperatures studied. At the higher temperature, ΔG° value becomes more negative (decreases in negative) revealing the increase in the feasibility of adsorption. It also gives an idea about whether the adsorption was physical or chemical. Since the physical adsorption has a free energy change in the range of 0 to -20 kJ/mol, the chemisorption have a range of -80 to -400 kJ/mol [28]. The calculated ΔG° values were found to be in the range between -4.6 to -12.7 kJ/mol at 100 mg/L concentration of all the adsorbents which indicates the physical adsorption dominating the adsorption process.

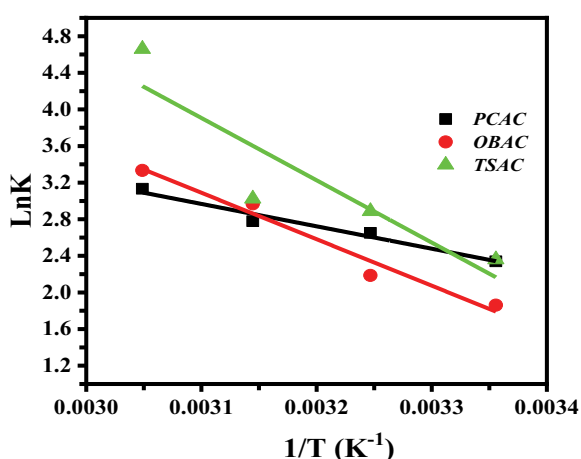


Fig. 14. Van't Hoff plot.

Table 7

Central composite design response of the removal efficiency of methylene blue for different parameters onto PCAC, OBAC, and TSAC

PCAC-MB				OBAC-MB				TSAC-MB			
A	B	C	R%	A	B	C	R%	A	B	C	R%
275.000	40.0000	318.000	88.0	275.000	40.0000	318.000	60.8	275.000	40.0000	318.000	86.9
275.000	40.0000	318.000	86.9	275.000	40.0000	318.000	61.0	275.000	40.0000	318.000	87.3
250.000	45.0000	323.000	89.0	250.000	45.0000	323.000	80.0	250.000	45.0000	323.000	91.4
300.000	45.0000	313.000	76.0	300.000	45.0000	313.000	46.0	300.000	45.0000	313.000	74.0
250.000	35.0000	323.000	89.3	250.000	35.0000	323.000	78.0	250.000	35.0000	323.000	89.3
275.000	40.0000	318.000	87.4	275.000	40.0000	318.000	60.5	275.000	40.0000	318.000	87.4
300.000	35.0000	323.000	77.0	300.000	35.0000	323.000	57.0	300.000	35.0000	323.000	68.7
300.000	45.0000	323.000	80.6	300.000	45.0000	323.000	59.0	300.000	45.0000	323.000	80.6
300.000	35.0000	313.000	64.0	300.000	35.0000	313.000	42.0	300.000	35.0000	313.000	63.6
275.000	48.4090	318.000	88.0	275.000	48.4090	318.000	62.0	275.000	48.4090	318.000	86.7
250.000	35.0000	313.000	86.0	250.000	35.0000	313.000	77.8	250.000	35.0000	313.000	87.0
317.045	40.0000	318.000	63.0	317.045	40.0000	318.000	47.7	317.045	40.0000	318.000	67.4
275.000	40.0000	318.000	88.0	275.000	40.0000	318.000	61.0	275.000	40.0000	318.000	87.0
250.000	45.0000	313.000	86.0	250.000	45.0000	313.000	71.9	250.000	45.0000	313.000	84.5
275.000	40.0000	318.000	87.6	275.000	40.0000	318.000	62.0	275.000	40.0000	318.000	86.4
275.000	31.5910	318.000	85.0	275.000	31.5910	318.000	59.9	275.000	31.5910	318.000	79.8
275.000	40.0000	318.000	87.0	275.000	40.0000	318.000	61.2	275.000	40.0000	318.000	87.2
275.000	40.0000	326.409	89.7	275.000	40.0000	326.409	76.8	275.000	40.0000	326.409	90.4
232.955	40.0000	318.000	89.0	232.955	40.0000	318.000	83.9	232.955	40.0000	318.000	88.6
275.000	40.0000	309.591	84.0	275.000	40.0000	309.591	53.0	275.000	40.0000	309.591	84.7

3.1.6. Experimental design and optimization

3.1.6.1. Comparison of ANOVA results of activated carbon

The results of the statistical analysis are shown in Tables 7–9. The experimental design for all the activated carbon for the removal of MB in percentage is shown in Table 7. From Table 8 it can be inferred that the P -value for all the activated carbon is within the significant limit ($P < 0.05$). The lack of fit value also indicates that the model fits well for dye removal by all the three activated carbon. The F -value was highest for the OBAC, followed by PCAC and TSAC. Each carbon has different efficiency for removing the dye. The P -value for the linear factor was also found to be significant within 95% significance.

The validity of the model was checked with the R^2 value. The Table 9 shows that the R^2 value for all the activated carbon is above 0.9. The adjusted R^2 is also above 0.9, suggesting that the model is well fitted for removing the dye using the activated carbon. The regression equation for removing the MB dye for each activated carbon from the CDD was presented from Eqs. (13)–(15).

The F -value of the linear factor showed that the dye concentration is the most significant for all the activated carbon. Regarding the significance of concentration, OBAC is the highest followed by PCAC and TSAC.

Interestingly, the time of contact between the dye and the adsorbent plays the least significant role. OBAC showed the least effect on time and was found to show a P -value of 0.517, indicating that the time is not statistically significant. On the other hand, TSAC showed greater significance

Table 8
ANOVA results for the model

Source	DF	PCAC-MB				OBAC-MB				TSAC-MB			
		Adj. SS	Adj. MS	F-value	P-value	Adj. SS	Adj. MS	F-value	P-value	Adj. SS	Adj. MS	F-value	P-value
Model	9	1,137.71	126.413	37.46	0.000	2,538.03	282.00	54.87	0.000	1,207.96	134.217	31.47	0.000
Linear	3	793.25	264.418	78.36	0.000	2,412.29	804.10	156.47	0.000	896.52	298.841	70.06	0.000
A	1	680.84	680.837	201.76	0.000	1,983.39	1,983.39	385.95	0.000	746.27	746.271	174.96	0.000
B	1	30.31	30.310	8.98	0.013	2.32	2.32	0.45	0.517	82.20	82.196	19.27	0.001
C	1	82.11	82.107	24.33	0.001	426.58	426.58	83.01	0.000	68.05	68.054	15.95	0.003
Square	3	287.44	95.812	28.39	0.000	60.62	20.21	3.93	0.043	241.59	80.530	18.88	0.000
A ²	1	285.81	285.813	84.70	0.000	39.16	39.16	7.62	0.020	206.35	206.353	48.38	0.000
B ²	1	7.91	7.914	2.35	0.157	0.06	0.06	0.01	0.914	53.56	53.562	12.56	0.005
C ²	1	5.49	5.492	1.63	0.231	25.50	25.50	4.96	0.050	2.39	2.394	0.56	0.471
2-Way	3	57.02	19.008	5.63	0.016	65.11	21.70	4.22	0.036	69.84	23.281	5.46	0.018
AB	1	31.60	31.601	9.36	0.012	12.25	12.25	2.38	0.154	64.41	64.411	15.10	0.003
AC	1	15.96	15.961	4.73	0.055	48.51	48.51	9.44	0.012	0.78	0.781	0.18	0.678
BC	1	9.46	9.461	2.80	0.125	4.35	4.35	0.85	0.379	4.65	4.651	1.09	0.321
Error	10	33.74	3.374			51.39	5.14			42.65	4.265		
LOF	5	32.62	6.523	28.91	0.001	50.10	10.02	38.89	0.001	42.00	8.400	64.29	0.000
PE	5	1.13	0.226			1.29	0.26			0.65	0.131		
Total	19	1,171.46				2,589.42				1,250.61			

Table 9
Model summary of the central composite design for the adsorption of methylene blue from wastewater by PCAC, OBAC, and TSAC

Adsorbent	S	R-sq.	R-sq. (Adj.)	R-sq. (Pred.)
PCAC	1.83697	97.12%	94.53%	77.66%
OBAC	2.26695	98.02%	96.23%	84.49%
TSAC	2.06529	96.59%	93.52%	74.36%

towards time than PCAC. OBAC behavior towards the effect of time was contrary to the other activated carbon. It can be attributed to the surface morphology of the activated carbon; with an increase in the number of pores and surface area, the time of contact becomes less significant. The temperature is the second most important factor for all the carbon after concentration. The order of significance of temperature was found to be OBAC > PCAC > TSAC.

The squared interaction of the variable was found to be significant overall for all the activated carbon, and the order of significance concerning the activated carbon was PCAC > TSAC > OBAC. Concentration squared was the most significant for all the carbon, and the order of significance was found to be the same as the overall squared interaction. Time squared was not significant for almost all carbon except for the small interaction effect shown by TSAC. Temperature squared was also the least significant for almost all carbon except for OBAC.

Two-way interactions were significant for all the activated carbon, with PCAC showing the highest significance, followed by TSAC and OBAC. The two-way interaction between the variable showed an interesting trend with concentration-time interaction significant for TSAC and

PCAC, while for OBAC, the interaction was insignificant. Interesting concentration temperature interaction was significant for OBAC only; other carbon does not show any significant interaction. Time-temperature interaction was found to be the least significant among the interactions, with no carbon showing any significance, and the *P*-value was greater than 0.05.

A 3D surface plot of the interaction between the two variables and the response is shown in Fig. 15. Three activated carbon shows the different trends in the interaction of two variables. The concentration of the adsorbent with a time of contact for PCAC and TSAC interaction along with the response was identical. With the increase in the dye concentration, the removal first increases and then subsequently there was a decrease in removal. This trend may be due to the fact at low concentration, competition for the active site would be less, and hence desorption may dominate; with the increase in concentration subsequently the competition for the active site increases and hence the adsorption increases [29]. But with a large increase in the dye, the active site would be completely occupied, and hence response decreases. It is interesting to note that PCAC and TSAC show a decrease in the removal of MB at low concentrations with an increase in time. Thereby, desorption predominates as the equilibrium shift towards desorption. With the increase in concentration, the equilibrium will shift towards the adsorption with an increase in time. But, OBAC shows a different trend; response increases with a decrease in concentration. Chemistry for the OBAC was found to be different as the equilibrium does not control the adsorption experiment. With the increase in time at low concentration, the adsorption was higher than the other activated carbon. In OBAC, as the increasing concentration decreases the removal, and an increase in time increases the removal of the dye.

In the case of the interaction of concentration, temperature with response showed the different trends for the carbon. PCAC response tends to increase with the increase in concentration at all temperatures and then subsequently decreases. The reason would be in the same line with the concentration-time relation. Adsorption increase with the

increase in concentration and then subsequently decreases. But response seems to decrease with an increase in temperature at lower concentrations since desorption plays an important role as physical adsorption decreases with an increase in temperature. OBAC shows an altogether different trend compared to the other two carbons. With the increase

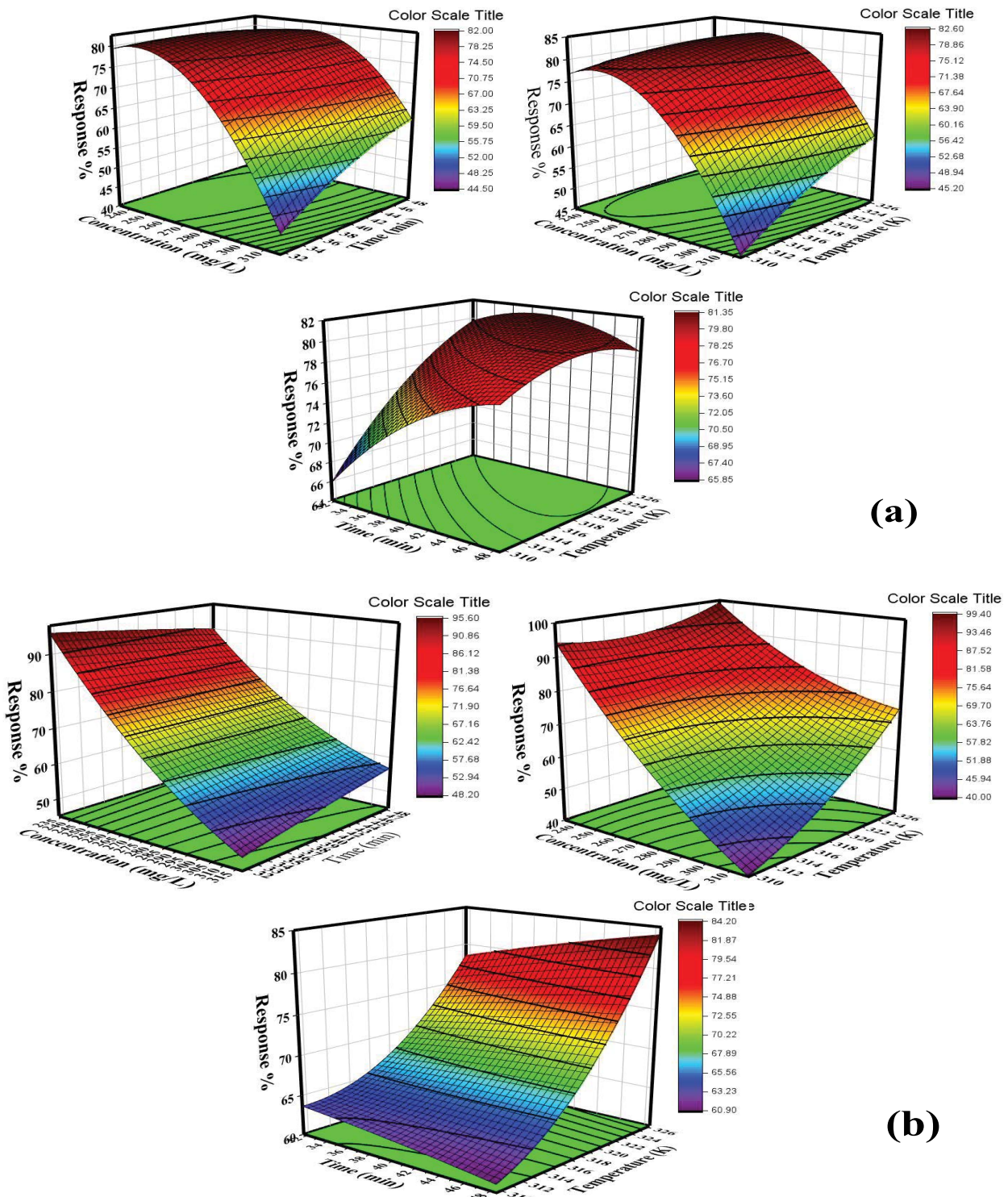
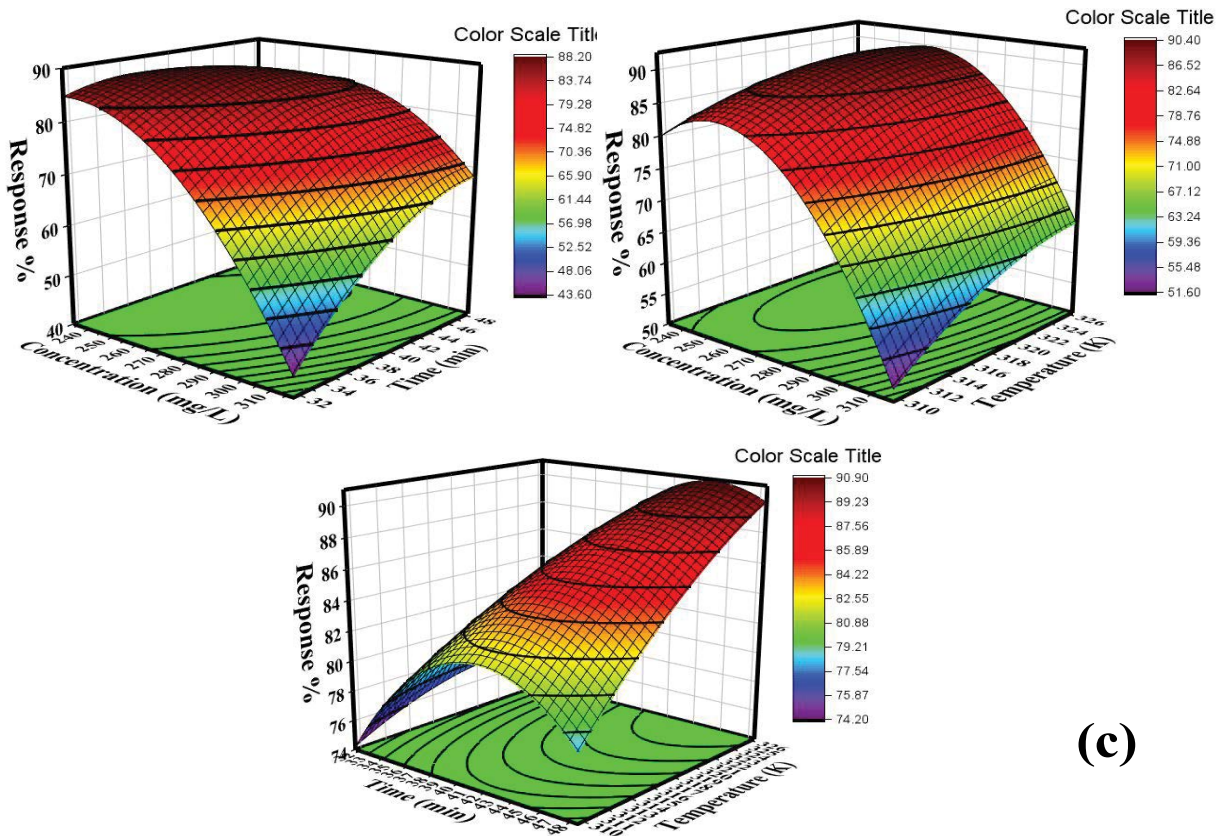


Fig. 15 (Continued)



(c)

Fig. 15. Surface plot of methylene blue (concentration – 275 mg/L; time – 40 min; temperature – 318 K).

in the concentration of the dye, the response decreases for all the temperatures. The lower concentration increase in temperature increases the adsorption compared to the other carbon. TSAC shows a mixed trend of the interaction of both PCAC and TSAC. With the increase in concentration, the adsorption decreases for all temperatures. But a concentration increase in temperature increases the removal of dye.

The interaction effect of time and temperature with response was found to be different for the carbon. PCAC with an increase in time at a lower temperature the removal increases but at a higher temperature with an increase in time, the removal decreases. OBAC shows interesting interaction as the temperature increased for the same time there was a large increase in the removal and the trend continues for all time. The effect of the interaction of time and temperature was found to be more profound in OBAC than in other carbon. In TSAC, at first, the response increases and then decreases for almost all temperatures with an increase in time. The optimum dye removal condition for 99% removal from the CCD model was shown in the Table 10 for each adsorbent. At a constant time with an increase in temperature, the response decreases at the low time, and at the high time, the removal increases with an increase in temperature. By solving the regression equation [Eqs. (14)–(16)] and analyzing the response surface contour plots, the optimum values of the operating variables can be determined [30]. Experiments were carried out to confirm the

optimum condition and experimental results are shown in Table 10.

$$R_{PCAC} \% = -2476 - 0.59A + 12.13B + 14.8C - 0.007125A^2 - 0.0296B^2 - 0.0274C^2 + 0.01590AB + 0.01130AC - 0.0435BC \tag{14}$$

$$R_{OBAC} \% = -7618 - 8.59A - 11.8B - 39.3C + 0.002638A^2 - 0.0027B^2 + 0.0532C^2 + 0.00990AB + 0.01970AC - 0.0295BC \tag{15}$$

$$R_{TSAC} \% = -1367 + 1.33A - 9.28B - 8.9C + 0.006054A^2 - 0.0771B^2 + 0.0163C^2 + 0.02270AB + 0.00250AC - 0.0305BC \tag{16}$$

where *A*, *B* and *C* are the coded values introduced as concentration, time, and temperature symbols used in experimental design.

In numerical optimization, the desired goal was for all the variables and responses from the optimization menu. The goal was set to maximize the response for all the carbons to analyze the viable optimal condition of the operating factors. Table 10 shows the predicted result obtained from the CCD model which coincides well with the experimental response for all the activated carbons, that indicates its feasibility and effectiveness for the adsorption of

Table 10
Response optimization of the factors using central composite design modeling and experimental results

Materials	Solution	A	B	C	Predicted response	Experimental response
PCAC	1	254.190	33.2898	326.409	92.0761	91.472
OBAC	1	232.955	31.5910	326.409	92.7465	92.021
TSAC	1	255.889	41.9536	326.409	93.0807	93.442

MB. It was found that the optimum concentrations (*A*), time (*B*), the temperature (*C*) of 254.19 mg/L, 33.29 min, 326.4 K, respectively for PCAC are with almost the same predicted and experimental response. OBAC has the 92.7% and 92.02% for predicted and experimental response with the resulting optimum conditions of *A* was 232.95 mg/L, *B* was 31.59 min, and *C* was 326.4 K. TSAC has the highest response for the removal of MB dye and also the predicted and experimental response was found to be concurrent. *A*, *B*, and *C* for TSAC were 255.89 mg/L, 41.95 min, and 326.4 K, respectively. The optimized result of CCD revealed that the optimum temperature was identical for all the activated carbon for the adsorption of MB dye from the aqueous solution. The order of the carbon with better response was TSAC > OBAC > PCAC for the adsorption of MB dye.

4. Conclusion

Three activated carbons from different plant sources were prepared using phosphoric acid activation, characterized, and removal efficiency toward methylene blue has been tested. The following conclusion was made from the study.

- FTIR studies showed that all the activated carbon indicated nearly the same functional group, but XRD and BET isotherm studies showed that these activated carbons had different morphology, and the same activation could form different morphological activated carbon.
- The study showed the adsorption of MB by all the carbon followed the Freundlich isotherm model, second-order kinetic model, and Weber Morris intraparticle diffusion model.
- The adsorption was found to be endothermic and physisorption dominated the removal rather than the chemisorption.
- RSM with the CCD model was found to fit the adsorption process and fitness follows the order TSAC > OBAC > PCAC.

References

- [1] S.K. Theydan, M.J. Ahmed, Adsorption of methylene blue onto biomass-based activated carbon by FeCl₃ activation: equilibrium, kinetics, and thermodynamic studies, *J. Anal. Appl. Pyrolysis*, 97 (2012) 116–122.
- [2] H. Li, L. Liu, J. Cui, J. Cui, F. Wang, F. Zhang, High-efficiency adsorption and regeneration of methylene blue and aniline onto activated carbon from waste edible fungus residue and its possible mechanism, *RSC Adv.*, 10 (2020) 14262–14273.
- [3] Z. Wang, M. Gao, X. Li, J. Ning, Z. Zhou, G. Li, Efficient adsorption of methylene blue from aqueous solution by graphene oxide modified persimmon tannins, *Mater. Sci. Eng., C*, 108 (2020) 110196, doi: 10.1016/j.msec.2019.110196.
- [4] N.C. Corda, M. Srinivas Kini, A review on adsorption of cationic dyes using activated carbon, *MATEC Web Conf.*, 144 (2018) 02022, doi: 10.1051/mateconf/201814402022.
- [5] D. Ghosh, K.G. Bhattacharyya, Adsorption of methylene blue on kaolinite, *Appl. Clay Sci.*, 20 (2002) 295–300.
- [6] M.A.K.M. Hanafiah, S.Z.M. Jamaludin, K. Khalid, S. Ibrahim, Methylene blue adsorption on *Aloe vera* rind powder: kinetics, isotherm and mechanisms, *Nat. Environ. Pollut. Technol.*, 17 (2018) 1055–1064.
- [7] V. Tharaneedhar, P. Senthil Kumar, A. Saravanan, C. Ravikumar, V. Jaikumar, Prediction and interpretation of adsorption parameters for the sequestration of methylene blue dye from aqueous solution using microwave assisted corncob activated carbon, *Sustainable Mater. Technol.*, 11 (2017) 1–11.
- [8] I.A.W. Tan, A.L. Ahmad, B.H. Hameed, Adsorption of basic dye on high-surface-area activated carbon prepared from coconut husk: equilibrium, kinetic and thermodynamic studies, *J. Hazard. Mater.*, 154 (2008) 337–346.
- [9] M.J. Ahmed, Application of agricultural based activated carbons by microwave and conventional activations for basic dye adsorption: review, *J. Environ. Chem. Eng.*, 4 (2016) 89–99.
- [10] M. Berrios, M.A. Martín, A. Martín, Treatment of pollutants in wastewater: adsorption of methylene blue onto olive-based activated carbon, *J. Ind. Eng. Chem.*, 18 (2012) 780–784.
- [11] N. Kashi, N.E. Fard, R. Fazaeli, Empirical modeling and CCD-based RSM optimization of Cd(II) adsorption from aqueous solution on clinoptilolite and bentonite, *Russ. J. Appl. Chem.*, 90 (2017) 977–992.
- [12] M. Koby, E. Demirbas, U. Gebologlu, M.S. Oncel, Y. Yildirim, Optimization of arsenic removal from drinking water by electrocoagulation batch process using response surface methodology, *Desal. Water Treat.*, 51 (2013) 6676–6687.
- [13] S. Porhemmat, M. Ghaedi, A.R. Rezvani, M.H.A. Azghandi, A.A. Bazrafshan, Nanocomposites: synthesis, characterization and its application to removal azo dyes using ultrasonic assisted method: modeling and optimization, *Ultrason. Sonochem.*, 38 (2017) 530–543.
- [14] R. Mostafaloo, M.H. Mahmoudian, M. Asadi-Ghalhari, BiFeO₃/magnetic nanocomposites for the photocatalytic degradation of cefixime from aqueous solutions under visible light, *J. Photochem. Photobiol., A*, 382 (2019) 111926, doi: 10.1016/j.jphotochem.2019.111926.
- [15] V. Gvoić, D.V. Kerkez, M. Prica, S. Rapajić, A.S.L. Maćerak, M. Bečelić-Tomin, D. Tomašević Pilipović, Optimization of Cyan flexo dye removal by nano zero-valent iron using response surface methodology, *J. Graphic Eng. Des.*, 8 (2017) 35–45.
- [16] M. Behbahani, M.R. Alavi Moghaddam, M. Arami, Techno-economical evaluation of fluoride removal by electrocoagulation process: optimization through response surface methodology, *Desalination*, 271 (2011) 209–218.
- [17] A. Nasrullah, A.H. Bhat, A. Naeem, M.H. Isa, M. Danish, High surface area mesoporous activated carbon-alginate beads for efficient removal of methylene blue, *Int. J. Biol. Macromol.*, 107 (2018) 1792–1799.
- [18] L. Li, X. Zhu, D. Yang, L. Gao, J. Liu, R. Vasant Kumar, J. Yang, Preparation and characterization of nano-structured lead oxide from spent lead acid battery paste, *J. Hazard. Mater.*, 203 (2012) 274–282.

- [19] J.-W. Lee, S.-P. Choi, R. Thiruvengatchari, W.-G. Shim, H. Moon, Evaluation of the performance of adsorption and coagulation processes for the maximum removal of reactive dyes, *Dyes Pigm.*, 69 (2006) 196–203.
- [20] M.H. Abdel-Aziz, E.Z. El-Ashtouky, M. Bassyouni, A.F. Al-Hossain, E.M. Fawzy, S.M.S. Abdel-Hamid, M.S. Zoromba, DFT and experimental study on adsorption of dyes on activated carbon prepared from apple leaves, *Carbon Lett.*, 31 (2021) 863–878.
- [21] P. Hadi, K.Y. Yeung, J. Barford, K.J. An, G. McKay, Significance of “effective” surface area of activated carbons on elucidating the adsorption mechanism of large dye molecules, *J. Environ. Chem. Eng.*, 3 (2015) 1029–1037.
- [22] M. Ghaedi, A. Ansari, F. Bahari, A.M. Ghaed, A. Vafaei, A hybrid artificial neural network and particle swarm optimization for prediction of removal of hazardous dye brilliant green from aqueous solution using zinc sulfide nanoparticle loaded on activated carbon, *Spectrochim. Acta, Part A*, 137 (2015) 1004–1015.
- [23] E. Fosso-Kankeu, H. Mittal, F. Waanders, S.S. Ray, Thermodynamic properties and adsorption behaviour of hydrogel nanocomposites for cadmium removal from mine effluents, *J. Ind. Eng. Chem.*, 48 (2017) 151–161.
- [24] M. Doğan, M. Alkan, A. Türkyilmaz, Y. Özdemir, Kinetics and mechanism of removal of methylene blue by adsorption onto perlite, *J. Hazard. Mater.*, 109 (2004) 141–148.
- [25] K. Shen, M.A. Gondal, Removal of hazardous Rhodamine dye from water by adsorption onto exhausted coffee ground, *J. Saudi Chem. Soc.*, 21 (2017) S120–S127.
- [26] M. Ghaedi, Comparison of cadmium hydroxide nanowires and silver nanoparticles loaded on activated carbon as new adsorbents for efficient removal of Sunset yellow: kinetics and equilibrium study, *Spectrochim. Acta, Part A*, 94 (2012) 346–351.
- [27] L.R. Bonetto, F. Ferrarini, C. de Marco, J.S. Crespo, R. Guégan, M. Giovanela, Removal of methyl violet 2B dye from aqueous solution using a magnetic composite as an adsorbent, *J. Water Process Eng.*, 6 (2015) 11–20.
- [28] Z. Bekçi, Y. Seki, L. Cavas, Removal of malachite green by using an invasive marine alga *Caulerpa racemosa var. cylindracea*, *J. Hazard. Mater.*, 161 (2009) 1454–1460.
- [29] F.S. Tabatabaei, M. Asadi-Ghalhari, R. Aali, F. Mohammadi, R. Mostafaloo, R. Esmaili, Z. Davarparast, Z. Safari, Removal of cefixime from water using rice starch by response surface methodology, *Avicenna J. Med. Biotechnol.*, 12 (2020) 230–235.
- [30] P. Agarwal, P.K. Mishra, P. Srivastava, Statistical optimization of the electrospinning process for chitosan/poly lactide nanofabrication using response surface methodology, *J. Mater. Sci.*, 47 (2012) 4262–4269.